Sensors and Actuators A 147 (2008) 279–285

Contents lists available at ScienceDirect

Sensors and Actuators A: Physical

journal homepage: www.elsevier.com/locate/sna

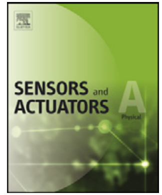

Effect of electrode size and silicon residue on piezoelectric thin-film membrane actuators

Cheng-Chun Lee [a], Qing Guo [a], G.Z. Cao [b], I.Y. Shen [a,*]

[a] Department of Mechanical Engineering, University of Washington, Seattle, WA 98195-2600, USA
[b] Department of Material Science & Engineering, University of Washington, Seattle, WA 98195-2120, USA

ARTICLE INFO

Article history:
Received 9 November 2007
Received in revised form 25 April 2008
Accepted 27 April 2008
Available online 4 May 2008

Keywords:
PZT thin films
Membrane actuators
Silicon residue
Electrode size
Finite element analysis

ABSTRACT

Piezoelectric micro-electromechanical systems (MEMS) often adopt a membrane structure to facilitate sensing or actuation. Design parameters, such as membrane size, thickness of the piezoelectric thin film, and electrode types, have been studied to maximize actuation, sensitivity, or coupling coefficient. This paper is to demonstrate numerically and experimentally that the size of silicon residue and its relative size to the top electrode are two critical yet unrecognized parameters in maximizing the actuation displacement of PZT thin-film membrane actuators. To study effects of the silicon residue, we have developed a finite element model using ANSYS. The model consists of five components: a square passive silicon membrane, a silicon substrate, a PZT thin film, a square top electrode, and a silicon residue region. In particular, the silicon residue has a circular inner diameter and a square outer perimeter with a trapezoidal cross section. Predictions of the finite element model lead to several major results. First, when the silicon residue is present, there exists an optimal size of the top electrode maximizing the actuator displacement. Second, the optimal electrode size is roughly 50–60% of the inner diameters of the silicon residue. The displacement of the membrane actuator declines significantly as the electrode overlaps with the silicon residue. Third, the maximal actuator displacement decreases as the inner diameter of the silicon residue decreases. Aside from the finite element analysis, a mechanics-of-material model is also developed to predict the electrode size that maximizes the actuator displacement. To verify the simulation results, eight PZT thin-film membrane actuators with progressive electrode sizes are fabricated. These actuators all have a square membrane of 800 μm × 800 μm with the inner diameter of the silicon residue controlled between 500 and 750 μm. A laser Doppler vibrometer is used to measure the actuator displacements. The experimental measurements confirm that there exists an optimal size of the top electrode maximizing the actuator displacement.

© 2008 Elsevier B.V. All rights reserved.

1. Introduction

PZT thin-film microactuators have a wide range of applications, such as scanning mirrors [1,2], hard disk drive read/write heads [3], micro pumps and valves [4,5], atomic force microscopes [6,7], and radio-frequency switches [8–10]. These microactuators usually take the form of cantilevers, bridges, and membranes.

For a PZT thin-film membrane actuator (Fig. 1), it typically consists of four parts: a membrane, a bulk silicon substrate, a PZT thin-film layer, and a pair of electrodes. The membrane is a moving component of the actuator anchored to the silicon substrate. As a result of its small thickness, the silicon membrane has low structural stiffness compared with the substrate. Often, the membrane can be fabricated by releasing part of the bulk silicon substrate. On top of the membrane is deposited a layer of PZT thin film with a pair of electrode. When a driving voltage is applied to the electrodes, the PZT thin film extends or contracts in the plane of the membrane, thus creating a bending moment that causes out-of-plane vibration of the membrane. Such PZT thin-film membrane actuators have appeared in many applications including micro pumps [11], deformable mirrors [12], acoustic transducers [13–15], energy harvesters [16], and hybrid cochlear implant actuators [17].

In fabricating PZT thin-film membrane actuators, silicon residues may result from an uneven etch rate while releasing the membrane from the substrate. In fact, the presence of silicon residues is desirable from the viewpoint of mechanical design, because silicon residues can reduce stress concentration and prolong the fatigue life. To illustrate the presence of silicon residues, Fig. 2 shows an SEM photo of the backside of a PZT thin-film membrane actuator. The membrane is not uniform in thickness as

* Corresponding author. Tel.: +1 206 543 5718; fax: +1 206 685 8047.
E-mail address: ishen@u.washington.edu (I.Y. Shen).

0924-4247/$ – see front matter © 2008 Elsevier B.V. All rights reserved.
doi:10.1016/j.sna.2008.04.015

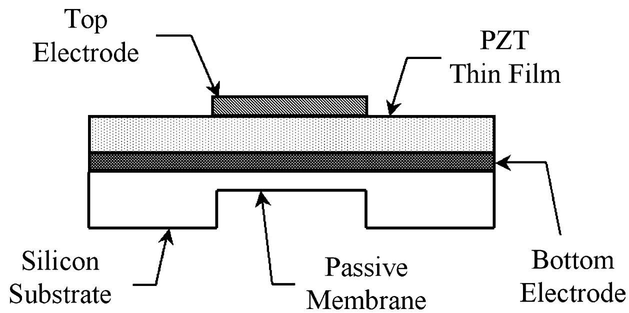

Fig. 1. Schematic drawing of PZT thin-film membrane actuator.

indicated by the color change in the SEM photo. Fig. 3 is a blowup of the corner between the membrane and the substrate, where the silicon residue appears in a triangular shape. Fig. 4 is an image of the backside of the membrane actuator under an optical microscope. The silicon residue appears in the form of small grains around the perimeter of the membrane. As evident from these experimental results, silicon residue is an important parameter that cannot be overlooked when designing PZT thin-film membrane microactuators.

To gauge the actuator performance, researchers have defined various performance indices (or objective functions) ranging from actuator displacement (or angle), quality factor, to electromechanical coupling coefficient. Design parameters studied thus far include material properties of PZT films, electrode design and coverage [18–22], membrane size and thickness [23,24], PZT film thickness [16], and residual stresses of the membrane layers [13,25,26]. Silicon residue, however, has never been considered as a design parameter, and its effects on actuator performance remain open.

This paper is to study how silicon residue affects actuator performance. In particular, silicon residue is considered as a design variable for optimization of the actuator displacement. In this paper, we first create a finite element model of the PZT thin-film membrane actuator including the silicon residue. With the finite element model, we study how the relative size of the electrode and the silicon residue affects the maximum displacement of the actuator. The finite element results also delineate physical mechanisms that maximize the actuator displacement. Finally, experiments are conducted to verify the finite element predictions.

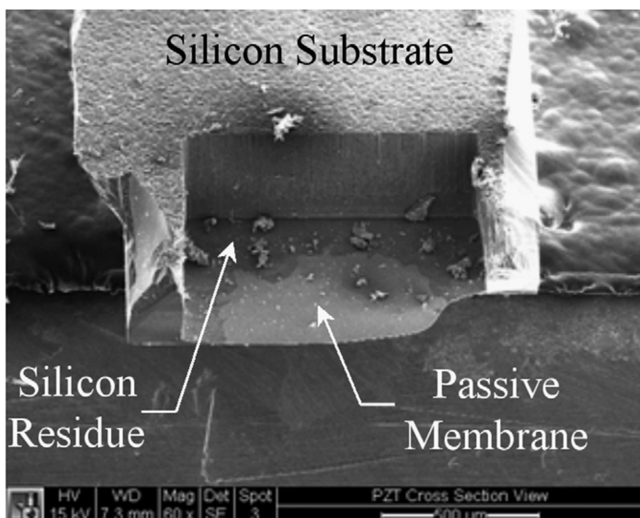

Fig. 2. SEM photo of the backside of a PZT thin-film membrane actuator.

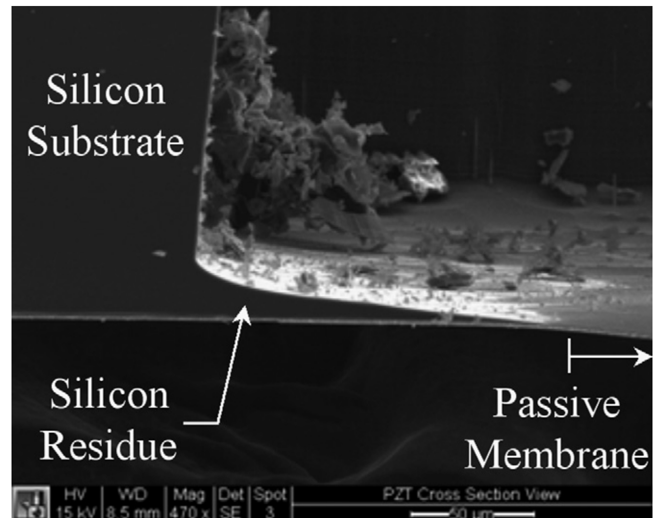

Fig. 3. SEM photo of the blowup of a silicon residue.

2. Finite element model

To study the effect of silicon residue on membrane actuators, a three-dimensional (3-D) finite element model is created with ANSYS; see Fig. 5. The finite element model consists of the following five components: a square passive membrane, a substrate, a PZT thin film, a square top electrode, and a silicon residue. The square passive membrane has width and length of 800 μm and thickness of 1 μm. The material of the passive membrane is silicon.

The substrate has dimensions of 3000 μm × 3000 μm with thickness of 400 μm. At the center of the substrate, a square hole of 800 μm × 800 μm is created to anchor the passive membrane. Moreover, boundary nodes of the passive membrane and the substrate are merged together such that the top surface of the passive membrane is flush with that of the substrate. The material of the substrate is also silicon.

To simplify the finite element model, the bottom electrode is not modeled separately. Instead, it is incorporated in the passive membrane and the substrate. This is a valid assumption, because the thickness of the bottom electrode is so tiny compared with that of the membrane itself (e.g., 0.05 μm of titanium and 0.1 μm of platinum vs. 1.0 μm of passive membrane). Similarly, isolation

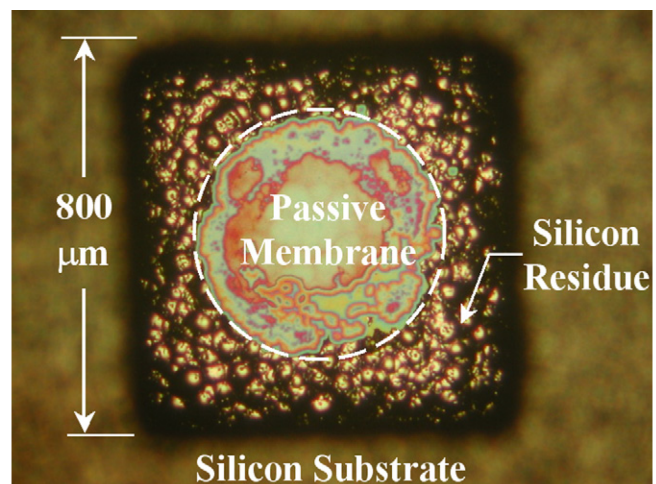

Fig. 4. Image of the silicon residue on the backside of the membrane actuator under an optical microscope.

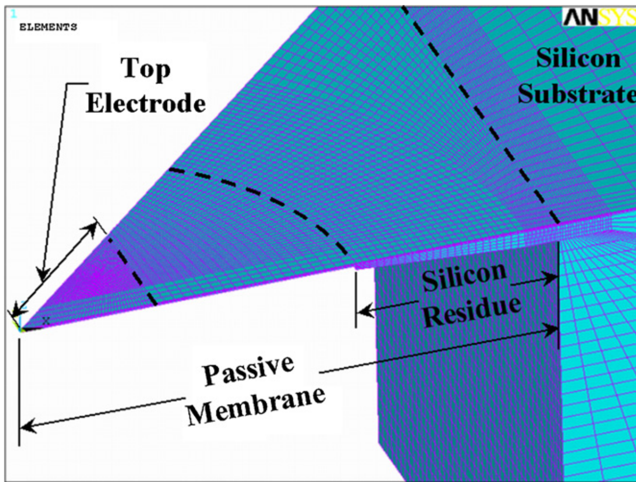

Fig. 5. Finite element model of the PZT thin-film membrane actuator.

layers, such as silicon oxide and nitride, are also incorporated in the passive membrane and the substrate to simplify the model.

In this finite element model, the PZT thin film has a thickness of 1 μm covering the silicon substrate and the passive membrane completely. The top electrode is square and has a thickness of 0.5 μm. Moreover, its areal dimensions vary from 200 μm × 200 μm to 1000 μm × 1000 μm in order to demonstrate the effects of the top electrode.

Finally, the silicon residue has a topology similar to a donut. The silicon residue has a circular inner circumference and a square outer circumference. The inner diameter of the silicon residue varies from 500 to 700 μm, as observed via an optical microscope (see Fig. 4). The outer circumference is a square of 800 μm × 800 μm. Moreover, the cross section of the silicon residue is trapezoidal with a constant slope angle measured from the SEM photo (Fig. 3). By maintaining the constant slope angle while varying the size of the inner diameter, we can create silicon residues of various volumes. Moreover, the silicon residue is located immediately below the passive membrane. In addition, the nodes of the upper surface of the silicon residue and the bottom surface of the passive membrane are merged together. The nodes of the silicon residue at the outer circumference and the nodes of the substrate at the inner circumference are also merged together.

Finally, all the components described above are meshed with solid elements. All the components, except the PZT thin film, are assumed to be linearly elastic. For the PZT thin film, its solid elements allow direct coupling effects of linear piezoelectricity. Moreover, material properties of a bulk PZT (PZT-4) are assumed, because exact material properties of PZT thin films remain unknown and can vary significantly depending on the quality of the film. For mechanical boundary conditions, the complete finite element model is constrained with geometrically fixed boundary conditions on the bottom surface of the silicon substrate. For electrical boundary conditions, an electric potential of 0 V is assigned to nodes at the top surface of the passive membrane and the substrate, where the bottom electrode is located. In addition, an electrical potential of 15 V is assigned to the interfacial nodes of the top electrode and the PZT film. A linear static analysis is conducted to predict the deflection of the center of the passive membrane for two reasons. First, the lowest natural frequency of this finite element model is above 100 kHz; therefore, harmonic responses of the actuator substantially below the first natural frequency is identical to that obtained from the static analysis. Second, the computational efforts of the static analysis are significantly less than those of a

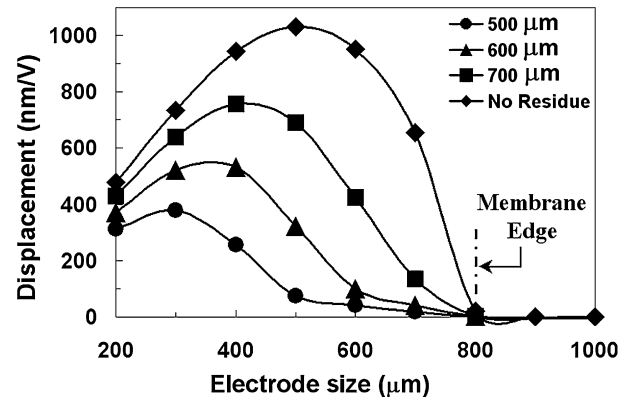

Fig. 6. Simulated displacement of the membrane actuators as a function of the top electrode size in view of various sizes of the silicon residue.

harmonic analysis. Due to the symmetry, only 1/8 of the actuator is modeled. Fig. 5 shows the final finite element model.

3. Results of the finite element analysis

Fig. 6 shows the simulated displacement of the membrane actuators as a function of the top electrode size. The top electrode varies in size from 200 to 1000 μm with a 100-μm increment. The actuator displacements are calculated for three different silicon residues, whose inner diameters are 500, 600, and 700 μm, respectively. In addition, the actuator displacements are calculated without a silicon residue as a reference.

There are several major results from Fig. 6. First, for a given size of silicon residue, there exists an optimal size of the top electrode that maximizes the actuator displacement. When the electrode is too small, the actuator displacement is small. When the size of the electrode exceeds the inner diameter of the silicon residue, the displacement also decreases significantly. When the size of the electrode exceeds the size of the passive membrane, the actuator displacement drops virtually to zero. Second, the optimal electrode size is roughly 50–60% of the inner diameter of the silicon residue. Third, the maximal actuator displacement decreases as the inner diameter of the silicon residue decreases. When the silicon residue is not present, the membrane actuator can reach the largest maximal actuator displacement.

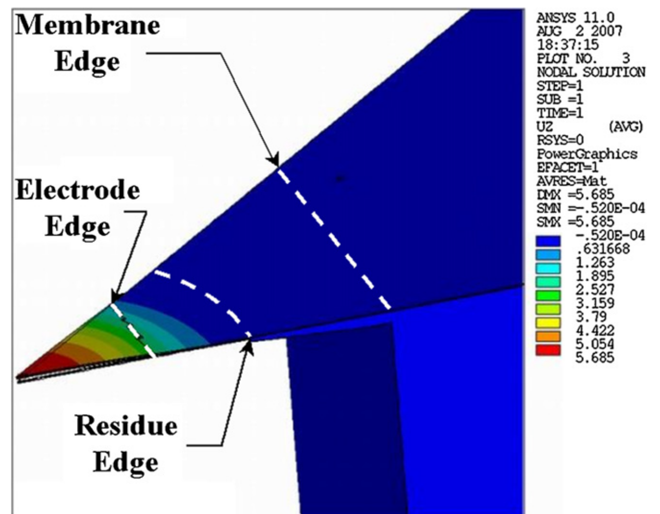

Fig. 7. Out-of-plane displacement distribution of membrane actuator when electrode size is smaller than the inner circumference of the residue.

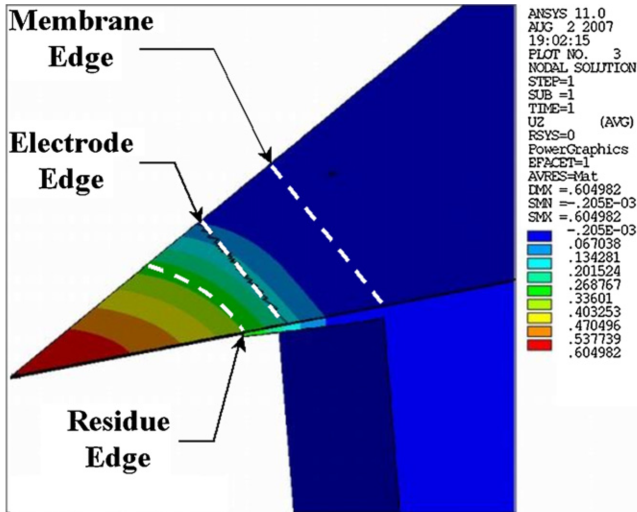

Fig. 8. Out-of-plane displacement distribution of membrane actuator when electrode size is larger than the inner circumference of the residue.

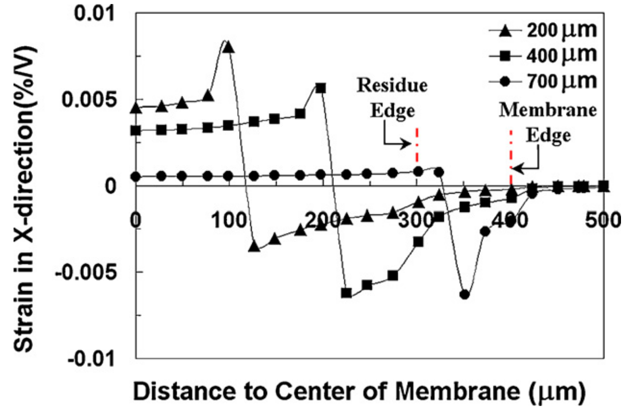

Fig. 10. In-plane strain of the membrane actuator along the centerline in Fig. 5 with three different electrode sizes.

Figs. 7 and 8 show two out-of-plane displacement distributions of the passive membrane with the electrode being smaller and larger than the inner diameter of the silicon residue, respectively. In either case, the displacement distribution is approximately axisymmetric indicating that the actuator displacement is primarily dominated by the geometry of the silicon residue rather than the geometry of the passive membrane or the electrode. Since the displacement field is roughly axisymmetric, we only need to analyze displacement or strain components along a line that passes through the center of the membrane in order to sort out physical mechanisms enhancing actuator performance.

Fig. 9 compares the out-of-plane displacement of the passive membrane along the centerline of the finite element model shown in Fig. 5 for three different electrode sizes. The inner diameter of the silicon residue is 600 μm. When the electrode is too small, (e.g., the electrode size being 200 μm × 200 μm), the displacement is localized at the center of the membrane and decreases rapidly far before reaching the silicon residue. Since the normal strain is proportional to the curvature of the membrane, the displacement field implies a large bending deformation localized at the center.

When the electrode is larger than the inner circumference of the silicon residue yet smaller than the passive membrane, (e.g., the electrode size being 700 μm × 700 μm), the displacement field is just the opposite. The displacement field does not vary significantly for most parts of the membrane until very close to the silicon residue. According to the curvature from the displacement field, the normal strain is small for most parts of the membrane. The electrode primarily deforms the silicon residue to result in the out-of-plane deflection. The deformation of the silicon residue, however, flattens the central portion of the passive membrane limiting the displacement.

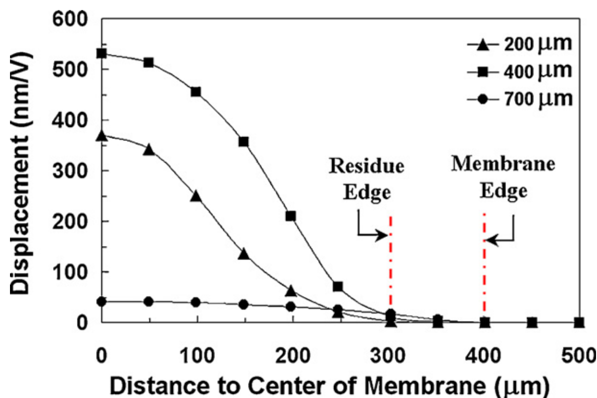

Fig. 9. Out-of-plane displacement of the membrane actuator along the centerline in Fig. 5 with three different electrode sizes.

Significant actuator displacements occur when the electrode size is large but not enough to exceed the inner diameter of the silicon residue (e.g., the electrode size being 400 μm × 400 μm). In this case, the portions inside and outside the electrode have roughly the same curvature according to the displacement field shown in Fig. 9.

The observation above can also be supported theoretically by analyzing the axial strain in the PZT thin film as follows. Fig. 10 shows the in-plane normal strain component ε_{xx} of the PZT thin film layer along the centerline (i.e., x axis) of the finite element model in Fig. 5. Let us focus for now on the strain distribution corresponding to electrode size of 400 μm × 400 μm. As stated above, this actuator generates significant displacement because of its optimal electrode size. There are several important things to note from its strain distribution.

First, the normal strain ε_{xx} experiences a sudden jump at the boundary of the electrode. According to the classical plate theory, in-plane normal strain component ε_{xx} is an indication of a bending moment. The sudden jump of ε_{xx} at the boundary of the electrode implies that the application of the electric potential difference is equivalent to a localized bending moment applied to the boundary of the electrode. As a result, the membrane inside and outside of the electrode bends in different directions. Although the strain ε_{xx} experiences a sudden jump across zero, the displacement field in Fig. 9 theoretically does not have an inflection point despite the fact that the displacement and slope remain continuous at the electrode boundary.

Second, the strain component ε_{xx} experiences a steep transition from the inner circumference of the silicon residue to the silicon substrate. This results from the change of bending rigidity of the silicon residue, as the thickness changes from the uniform membrane to the trapezoidal silicon residue. This gradual change will theoretically reduce stress concentration and prolong the fatigue life.

Third, the strain is tensile (i.e., positive) inside the electrode and compressive (i.e., negative) outside the electrode. For electrodes generating a significant actuator displacement (e.g., the 400 μm × 400 μm electrode), the positive strain and negative strain are about the same in magnitude. For small electrodes that do

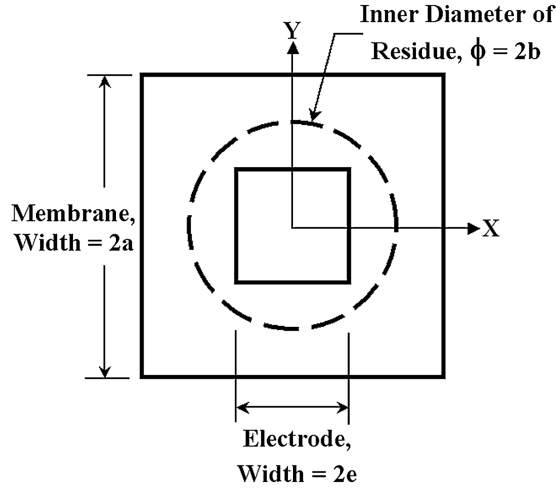

Fig. 11. Mechanics-of-material model of a membrane actuator.

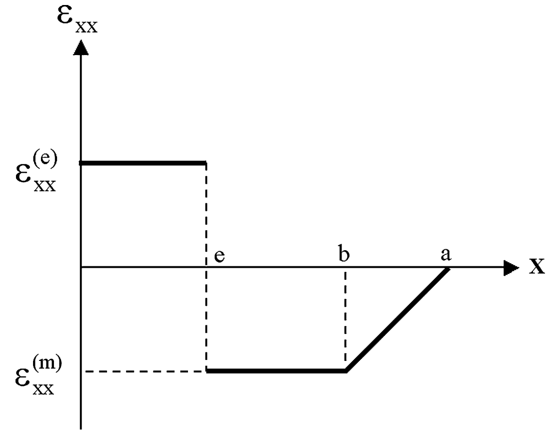

Fig. 12. Approximation of in-plane normal strain distribution in the X-direction for analytical model in Fig. 11.

not generate a significant displacement (e.g., the 200 μm × 200 μm electrode), the positive strain is significantly larger than the negative strain as far as the magnitude is concerned. This is consistent with the displacement field shown in Fig. 9 as we have explained above.

4. Predictions of optimal electrode size

The optimal electrode size to maximize actuator displacement can be predicted analytically through use of a simple mechanics-of-materials model as follows.

Let $2a$ be the length of the membrane, $2b$ be the inner diameter of the silicon residue, and $2e$ be the length of the electrode; see Fig. 11. Then $x = 0$ and $x = a$ correspond to the center and the edge of the membrane, respectively. According to linear elasticity,

$$\varepsilon_{xx} \equiv \frac{\partial u}{\partial x} \tag{1}$$

where $u(x)$ is the in-plane displacement of the PZT thin film in the x direction. Moreover, $u(x)$ is subjected to the following boundary conditions

$$u(0) = u(a) = 0 \tag{2}$$

In Eq. (2), $u(0) = 0$ results from the symmetry of the finite element model, whereas $u(a) = 0$ results from the fact that the membrane is anchored at the substrate. With (1) and (2),

$$\int_0^a \varepsilon_{xx}\,\mathrm{d}x = u(a) - u(0) = 0 \tag{3}$$

which implies that the area under each strain distribution ε_{xx} is summed to zero. In addition, let us define $\varepsilon_{xx}^{(e)}$, $\varepsilon_{xx}^{(m)}$, and $\varepsilon_{xx}^{(s)}$ as the normal strain in the PZT layer inside the electrode, outside the electrode, and within the silicon residue, respectively. In other words,

$$\varepsilon_{xx} \equiv \begin{cases} \varepsilon_{xx}^{(e)}, & 0 < x < e \quad \text{(inside electrode)} \\ \varepsilon_{xx}^{(m)}, & e < x < b \quad \text{(outside electrode)} \\ \varepsilon_{xx}^{(s)}, & b < x < a \quad \text{(within silicon residue)} \end{cases} \tag{4}$$

Considering the strain distributions obtained from the finite element analysis (e.g., Fig. 10), we may assume in this mechanics-of-material model that $\varepsilon_{xx}^{(e)}$ and $\varepsilon_{xx}^{(m)}$ are constant as a first approximation; see Fig. 12. Physically, this assumption implies that each of the two regions inside and outside the electrode is in pure bending with its respective bending moment. Moreover, $\varepsilon_{xx}^{(s)}$ is approximated as a linear function in x taking the form of

$$\varepsilon_{xx}^{(s)} = \frac{\varepsilon_{xx}^{(m)}}{a-b}(a-x), \quad b < x < a \tag{5}$$

Substitution of Eq. (4) into Eq. (3) results in

$$\varepsilon_{xx}^{(e)} e + \varepsilon_{xx}^{(m)}(b-e) + \int_b^a \varepsilon_{xx}^{(s)}\,\mathrm{d}x = 0 \tag{6}$$

Or, alternatively,

$$\left|\frac{\varepsilon_{xx}^{(e)}}{\varepsilon_{xx}^{(m)}}\right| = \frac{b-e}{e} + \frac{1}{e}\frac{\int_b^a \varepsilon_{xx}^{(s)}\,\mathrm{d}x}{\varepsilon_{xx}^{(m)}} \tag{7}$$

Substitution of Eq. (5) into Eq. (7) gives

$$\left|\frac{\varepsilon_{xx}^{(e)}}{\varepsilon_{xx}^{(m)}}\right| \approx \frac{b-e}{e} + \frac{a-b}{2e} \tag{8}$$

If the electrode size is 200 μm × 200 μm ($e = 100$ μm), the inner diameter of the silicon residue is 600 μm ($b = 300$ μm), and the membrane is 800 μm × 800 μm ($a = 400$ μm), calculations using (8) indicate that the strain inside the electrode is 2.5 times of the strain outside the electrode. This is consistent with the strain distribution shown in Fig. 10.

Eq. (6) can also be used to estimate the electrode size to maximize the actuator displacement. According to Fig. 9 and the discussion above, the maximal actuator displacement occurs when all portion of the membrane deforms with about the same curvature, i.e., $\left|\varepsilon_{xx}^{(e)}\right| \approx \left|\varepsilon_{xx}^{(m)}\right|$. Therefore, Eq. (7) indicates that the maximal actuator displacement occurs roughly around

$$\frac{e}{b} \approx \frac{1}{2} + \frac{1}{2b}\frac{\int_b^a \varepsilon_{xx}^{(s)}\,\mathrm{d}x}{\varepsilon_{xx}^{(m)}} \tag{9}$$

Eq. (9) is very useful in estimating the size of the electrode to produce the maximal actuator displacement. First of all, e/b in Eq. (9) has a lower bound of 0.5, which implies that the electrode size needs to be at least half of the inner diameter of the silicon residue in order to produce the maximal displacement. To further estimate e/b, let us substitute $\varepsilon_{xx}^{(s)}$ of Eq. (5) into Eq. (9) to obtain

$$\frac{e}{b} \approx \frac{1}{2} + \frac{1}{4}\left(\frac{a}{b} - 1\right) \tag{10}$$

As an example, let us consider a square membrane of 800 μm × 800 μm. The silicon residue has an inner diameter of

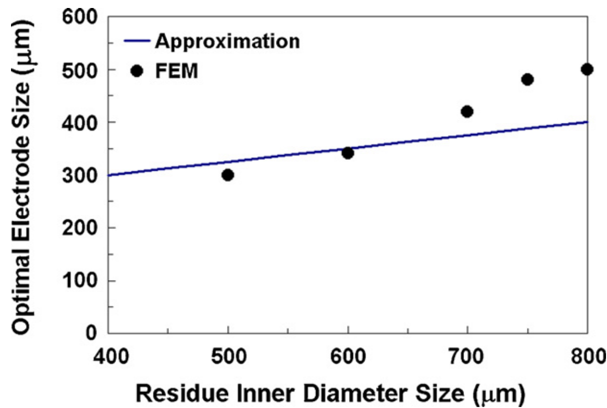

Fig. 13. Comparison of optimal electrode sizes from the analytical approximation and FEM data.

600 μm. In this case, a = 400 μm and b = 300 μm. Eq. (10) estimates that the maximal displacement occurs when $e/b \approx 58\%$. Fig. 13 compares the optimal electrode size e/b as calculated from the finite element analysis (Fig. 6) and from the mechanics-of-materials model (10). The two results agree well with each other, except when the inner diameter of the silicon residue exceeds 700 μm. As the inner diameter of the silicon residue approaches the size of the membrane, the silicon residue diminishes rapidly. As a result, the displacement field is dominated by the square shape of the membrane and is no longer axisymmetric. Thus, Eq. (10) loses its accuracy, because the assumption of an axisymmetric displacement field is no longer valid.

5. Experimental verification

An experiment was conducted to validate the finite element analysis. A 3 in. wafer with 32 membrane actuators was fabricated using the following procedure.

The silicon substrate (Si wafers with 400-μm thickness) is first oxidized in a furnace at 1045 °C for 3 h to grow a SiO_2 layer of 5000 Å thick. Then a layer of silicon nitride of 2000 Å thick is deposited by LPCVD (low-pressure chemical vapor deposition). The bottom electrode consists of Pt/Ti layers with thicknesses of 100 nm and 50 nm, respectively. The PZT film is spin-coated three times. For each coating, the sintering temperature is 650 °C for 15 min. Next, the top electrode consists of Au/Cr layers through evaporation. Finally, the backside of the silicon substrate is patterned and etched with deep reactive ion etching (DRIE) to form the suspension.

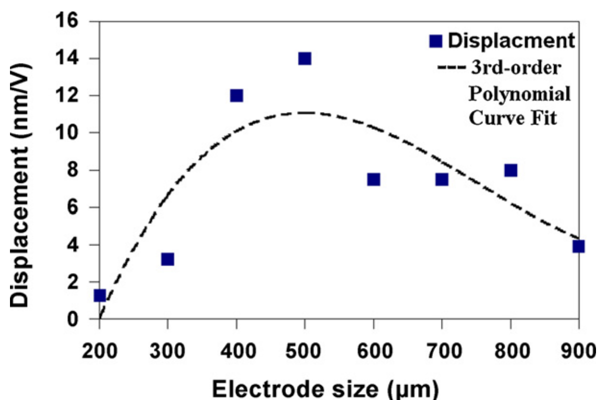

Fig. 14. Experimental displacement of the membrane actuators as a function of the top electrode size.

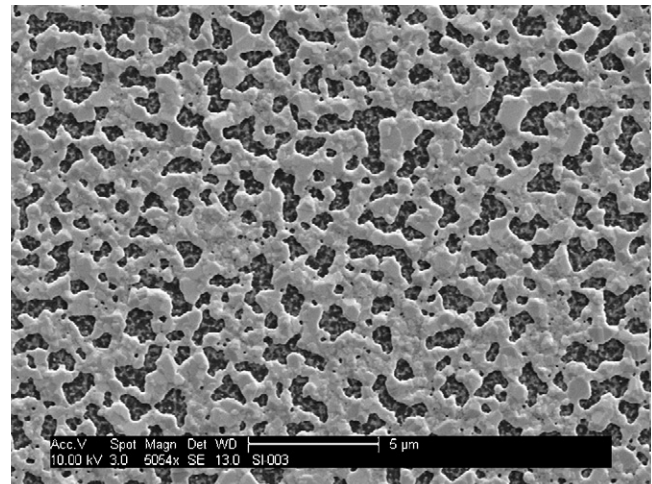

Fig. 15. Porous surface of bottom electrode.

Each membrane actuator has a passive membrane of 800 μm × 800 μm. The electrode size of these membrane actuators varies from 200 to 900 μm in a 100-μm increment. The backside of each actuator was inspected under an optical microscope to measure the inner diameter of its silicon residue. The measured inner diameters of the silicon residue vary from 500 to 750 μm.

The membrane actuators were first poled with 10 V for 30 min. A 3-kHz sinusoidal voltage with amplitude of 5 V was used to drive the actuators. A laser Doppler vibrometer (LDV) measured the displacement of the membrane actuator at the center of the top electrode. Fig. 14 illustrates the measured displacements with respect to the size of the top electrode. A third-order polynomial curve fit confirms that there is an optimal size of the top electrode maximizing the actuator displacement. Moreover, the optimal electrode size is roughly around 400–500 μm, which is about 60% of the size of the passive membrane.

The measured displacements, however, are significantly smaller than those predicted from the finite element analysis. For example, the measured displacement is in the order of 70 nm, whereas the finite element prediction is around 3–6 μm. The quantitative discrepancies may result from the following sources.

First, material constants of bulk PZT are used in the finite element analysis for the PZT thin film, because material properties of PZT thin films can hardly be measured. Since the piezoelectric properties of PZT thin films are known to be inferior to those of the bulk PZT, the finite element analysis will over-predict the displacement of the PZT thin-film membrane actuator. Second, exact thicknesses of the PZT layer and the silicon layer of the membrane are unknown in the experimental measurements. Therefore, the dimensions used in the finite element analysis are rough estimation based on previous thickness measurements from similar fabrication. Third, the piezoelectric properties of the PZT thin film depend significantly on the poling electrical field. In this set of experiments, the PZT film might have not been poled enough to reach its best performance. Finally, the bottom electrode is indeed porous not covering the entire substrate as a result of annealing; see Fig. 15. The presence of porosity reduces the effective area of the bottom electrode and consequently the actuator displacement.

6. Conclusions

We have developed a finite element model and conducted an experiment to study the effect of the silicon residue on PZT thin-film membrane actuators. The finite element analysis predicts three

major results. First, for a given size of the silicon residue, there exists an optimal size of the top electrode maximizing the actuator displacement. Second, the maximal displacement decreases as the inner diameter of the silicon residue decreases. Third, the optimal electrode size is roughly 50–60% of that inner diameter of the residue. This result has also been predicted analytically through use of a mechanics-of-material model with a reasonable accuracy. The actuator has virtually zero displacement when the size of the electrode equals or exceeds that of the silicon membrane. The experiment verifies the existence of a maximal displacement in different electrode sizes. The maximal displacement occurs when the top electrode size is about 60% of that of the passive membrane.

References

[1] W. Lin, A. Schroth, S. Matsumoto, C. Lee, R. Maeda, Two-dimensional microscanner actuated by PZT thin film, Proceedings of the SPIE 3892 (1999) 133–140.
[2] A. Schroth, C. Lee, S. Matsumoto, R. Maeda, Application of sol-gel deposited thin PZT film for actuation of 1D and 2D scanners, Sensors and Actuators A (Physical) A73 (March) (1999) 144–152.
[3] K. Suzuki, R. Maeda, J.R. Chu, T. Kato, M. Kurita, An active head slider using a piezoelectric cantilever for in situ flying-height control, IEEE Transactions on Magnetics 39 (2) (2003) 826–831.
[4] R. Maeda, J. Tsaur, S. Lee, M. Ichiki, Piezoelectric microactuator devices, Journal of Electroceramics 12 (2004) 89–100.
[5] J. Akedo, M. Lebedev, Fabrication of microfluidic-device (diffuser or mixer) using aerosol deposition method, Proceedings of SPIE – The International Society for Optical Engineering 4936 (2002) 234–240.
[6] S. Watanabe, T. Fujii, Micro-fabricated piezoelectric cantilever for atomic force microscopy, Review of Scientific Instruments 67 (November) (1996) 3898–3903.
[7] T. Itoh, T. Suga, Development of a force sensor for atomic force microscopy using piezoelectric thin films, Nanotechnology 4 (October) (1993) 218–224.
[8] S. Gross, S. Tadigadapa, T. Jackson, S. Trolier-McKinstry, Q. Zhang, Lead-zicornate-tinanate-based piezoelectric micromachined switch, Applied Physics Letter 83 (1) (2003) 174–176.
[9] H. Jiang, P. Kirby, Q. Zhang, Fabrication of PZT actuated cantilevers on silicon-on-insulator wafers for a RF microswitch, Proceedings of SPIE – The International Society for Optical Engineering 4979 (January) (2003) 165–173.
[10] C. Fox, X. Chen, H. Jiang, P. Kirby, S. McWilliam, Development of micro-machined RF switches with piezofilm actuation, Proceedings of SPIE – The International Society for Optical Engineering 4700 (March) (2002) 40–49.
[11] K. Brooks, D. Damjanovic, A. Kholkin, I. Reaney, N. Setter, P. Luginbuhl, G. Racine, N.F. De Rooij, A. Saaman, PZT films for micro-pumps, Integrated Ferroelectrics 8 (1) (1995) 13–23.
[12] Y. Hishinuma, E. Yang, Piezoelectric unimorph microactuator arrays for single-crystal silicon continuous-membrane deformable mirror, Journal of Microelectromechanical Systems 15 (2) (2006) 370–379.
[13] S. Ko, Y. Kim, S. Lee, S. Choi, S. Kim, Piezoelectric membrane acoustic devices, in: The 15th IEEE International Conference on Micro Electro Mechanical Systems, 2002, pp. 296–299.
[14] T. Ren, Y. Zhu, Y. Yang, X. Wu, N. Zhang, L. Lin, Z. Li, Micro acoustic devices using piezoelectric films, Intergrated Ferroelectrics 80 (2006) 331–340.
[15] J. Baborowski, M. Ledermann, P. Muralt, Piezoelectric micromachined ultrasonic transducers based on PZT films, Proceedings of Materials Research Society Symposium 741 (2002) 273–278.
[16] J. Cho, M. Anderson, R. Richards, D. Bahr, C. Richards, Optimization of electromechanical coupling for a thin-film PZT membrane: II. Experiment, Journal of Micromechanics and Microengineering 15 (2005) 1804–1809.
[17] C. Lee, C. Hume, G. Cao, I. Shen, A feasibility study of PZT thin-film microactuators for hybrid cochlear implants, in: Proceedings of the 2005 27th Annual International Conference of the Engineering in Medicine and Biology Society, IEEE-EMBS 2005, vol. 7, 2005, pp. 1929–1932.
[18] H. Choi, A. Dalakoti, S. Bose, A. Bandyopadhyay, Influence of top electrode design on pMUTs performance, Sensors and Actuators A 135 (2007) 613–619.
[19] E. Hong, S. Trolier-McKinstry, R. Smith, S. Krishnaswamy, C. Freidhoff, Design of MEMS PZT circular diaphragm actuator to generate large deflections, Journal of Micromechanics and Microengineering 15 (4) (2006) 832–839.
[20] C. Mo, R. Wright, W. Slaughter, R. Clark, Behaviour of a unimorph circular piezoelectric actuator, Smart Materials & Structures 15 (4 (August)) (2006) 1094–1102.
[21] C. Mo, R. Wright, W. Clark, The effect of electrode pattern on the behavior of piezoelectric actuators in a circular diaphragm structure, Journal of Intelligent Materials Systems and Structures 18 (5 (May)) (2007) 467–476.
[22] E. Yang, Y. Hishinuma, J. Cheng, S. Trolier-McKinstry, E. Bloemhof, B. Levine, Thin-film piezoelectric unimorph actuator-based deformable mirror with a transferred silicon membrane, Journal of Microelectromechanical Systems 15 (5 (October)) (2006) 1214–1225.
[23] J. Park, S. Yang, K. Lee, S. Kang, Fabrication and electro-mechanical characteristics of piezoelectric micro bending actuators on silicon substrates, Journal of the Ceramic Society of Japan 114 (11 (November)) (2006) 1089–1092.
[24] F. Akasheh, J. Fraser, S. Bose, A. Bandyopadhyay, Piezoelectric micromachined ultrasonic transducers: modeling the influence of structural parameters on device performance, IEEE Transaction on Ultrasonics, Ferroelectrics, and Frequency Control 52 (3 (March)) (2005) 455–468.
[25] H. Zhu, J. Miao, B. Chen, Z. Wang, W. Zhu, Membrane microcantilever arrays fabrication with PZT thin films for nanorange movement, Microsystem Technologies 11 (August) (2005) 1121–1126.
[26] S. Lee, R. Ried, R. White, Piezoelectric cantilever microphone and microspeaker, Journal of Microelectromechanical Systems 5 (4 (December)) (1996) 238–242.